ARTICLE

OPEN

Check for updates

Localized-to-itinerant transition preceding antiferromagnetic quantum critical point and gapless superconductivity in CeRh$_{0.5}$Ir$_{0.5}$In$_5$

Shinji Kawasaki[1✉], Toshihide Oka[1], Akira Sorime[1], Yuji Kogame[1], Kazuhiro Uemoto[1], Kazuaki Matano[1], Jing Guo[2], Shu Cai[2], Liling Sun[2], John L. Sarrao[3], Joe D. Thompson[3] & Guo-qing Zheng[1,2✉]

A fundamental problem posed from the study of correlated electron compounds, of which heavy-fermion systems are prototypes, is the need to understand the physics of states near a quantum critical point (QCP). At a QCP, magnetic order is suppressed continuously to zero temperature and unconventional superconductivity often appears. Here, we report pressure (P)-dependent ^{115}In nuclear quadrupole resonance (NQR) measurements on heavy-fermion antiferromagnet CeRh$_{0.5}$Ir$_{0.5}$In$_5$. These experiments reveal an antiferromagnetic (AF) QCP at $P_c^{AF} = 1.2$ GPa where a dome of superconductivity reaches a maximum transition temperature T_c. Preceding P_c^{AF}, however, the NQR frequency ν_Q undergoes an abrupt increase at $P_c^* = 0.8$ GPa in the zero-temperature limit, indicating a change from localized to itinerant character of cerium's f-electron and associated small-to-large change in the Fermi surface. At P_c^{AF} where T_c is optimized, there is an unusually large fraction of gapless excitations well below T_c that implicates spin-singlet, odd-frequency pairing symmetry.

[1] Department of Physics, Okayama University, Okayama 700-8530, Japan. [2] Institute of Physics, Chinese Academy of Sciences, Beijing National Laboratory for Condensed Matter Physics, Beijing 100190, China. [3] Los Alamos National Laboratory, Los Alamos, NM 87545, USA. ✉email: kawasaki@science.okayama-u.ac.jp; gqzheng123@gmail.com

Understanding non-Fermi liquid behaviors[1,2] due to a zero-temperature magnetic transition, a QCP, and the unconventional superconductivity that emerges around it is one of the central issues in condensed matter physics. These phenomena are widely seen in strongly correlated electron systems such as heavy fermion systems[1], cuprates[3], and iron pnictides[4,5]. In cuprates, iron pnictides, or other compounds containing $3d$ transition-metal elements[6], the quantum phase transition is described by itinerant spin-density wave (SDW) theories, where the QCP is due to an instability of the underlying large Fermi surfaces[7–10]. Cerium(Ce)-based heavy fermion systems are understood based on the Kondo lattice model in which localized Ce $4f$ electron spins at high temperatures are screened below a characteristic temperature T_K by the conduction electrons[11]. At high temperatures, the f electron spins are localized, and thus, the Fermi surface is small. With decreasing temperature, $4f$ electrons couple with the conduction electrons through Kondo hybridization, and the Fermi-surface volume gradually increases with decreasing temperature[12,13]. In addition to the Kondo effect, there also is a long-range Ruderman–Kittel–Kasuya–Yosida (RKKY) interaction that is the indirect exchange interaction among weakly screened, nearly localized $4f$ electrons. If the RKKY interaction overcomes the Kondo effect, f spins order antiferromagnetically below the Néel temperature T_N. By tuning a nonthermal control parameter such as pressure and/or chemical substitution, T_N can be suppressed completely to zero, and T_K increases as the parameter increases[11]. A crossover from the small (localized) to the large (itinerant) Fermi surfaces will occur well below T_K in the Kondo lattice[14]. Depending on the relative balance between Kondo hybridization and the RKKY interaction, magnetic order may be of the SDW-type or the RKKY-type antiferromagnetic (AF) order that is mediated by itinerant electrons of a small Fermi surface. Quantum criticality of the latter type of magnetic order is predicted theoretically to be qualitatively different from SDW criticality and involves a breakdown of Kondo screening and a transition from small-to-large Fermi surfaces at the QCP[10,15,16]. In practice, it can be difficult experimentally to distinguish unambiguously between these two scenarios, though distinctions have been inferred from combinations of thermodynamic, transport and inelastic neutron scattering measurements[17]. Unfortunately, it has not been possible to perform neutron scattering experiments under high pressure conditions, the "cleanest" tuning parameter that does not introduce additional disorder or break symmetry, to shed light on the nature of criticality in Kondo lattice systems. In contrast, pressure-dependent nuclear quadrupole resonance (NQR) measurements, which probe the dynamic spin susceptibility as well as the influence of Kondo hybridization, are straightforward, even at very low temperatures, and, as we show, can be used as differentiating probe of quantum criticality.

The AF superconductor CeRh$_{0.5}$Ir$_{0.5}$In$_5$[18,19] is a good candidate to investigate this issue. CeRhIn$_5$ has a small Fermi surface[20], orders antiferromagnetically below $T_N = 3.8$ K, and exhibits pressure-induced superconductivity above $P = 1.6$ GPa at the transition temperature $T_c = 2.1$ K[21]. T_c increases to 2.3 K at 2.35 GPa where, in the limit of zero temperature, there is a magnetic–nonmagnetic transition[22,23] accompanied by a change from small-to-large Fermi surface[20]. The superconducting-gap symmetry is consistent with d-wave symmetry[24,25]. On the other hand, CeIrIn$_5$ has a large Fermi surface[26], and also shows d-wave superconductivity below $T_c = 0.4$ K[27–29], which increases to 0.8 K at $P = 2.1$ GPa[30]. The alloyed compound CeRh$_{0.5}$Ir$_{0.5}$In$_5$ orders antiferromagnetically below $T_N = 3.0$ K at $P = 0$[31] and becomes superconducting below $T_c = 0.9$ K[18,19,32]. CeRh$_{0.5}$Ir$_{0.5}$In$_5$ is closer to an AF QCP than CeRhIn$_5$, suggesting that Ir substitution for Rh acts a positive chemical pressure. This suggestion can be

understood by appreciating that underlying the evolution of ground states in the CeRh$_{1-x}$Ir$_x$In$_5$ series is a systematic change in orbital anisotropy of the Γ_7^2 crystal-electric field ground state wave function that produces progressively stronger hybridization with increasing x[33].

Here, we report the results of ^{115}In-NQR measurements on CeRh$_{0.5}$Ir$_{0.5}$In$_5$ under pressure, crystal structure analysis and a first-principle calculation of NQR frequency ν_Q (see "Methods" for details). From the temperature dependence of the nuclear spin-lattice relaxation rate $(1/T_1)$, we find that the AF QCP is at $P_c^{AF} = 1.2$ GPa, where $T_c(P)$ reaches its maximum. From the pressure dependence of ν_Q, we find a localized-to-itinerant transition at $P_c^* = 0.8$ GPa before the AF QCP appears. Superconductivity is not only optimized at the AF QCP but also is realized with a remarkable proliferation of residual gapless excitations. Our results suggest that the large Fermi surface and AF instabilities in the presence of "impurity" scattering trigger unconventional gapless superconductivity in CeRh$_{0.5}$Ir$_{0.5}$In$_5$.

Results

The hyperfine coupling constant at the In(1) site. The hyperfine coupling between nuclear and electronic spins relates the measured $1/T_1$ to the underlying dynamical spin susceptibility as discussed in "Methods". Figure 1 shows the pressure–temperature phase diagram of the CeRh$_{1-x}$Ir$_x$In$_5$ system. If substituting Ir for Rh acts as a positive chemical pressure, we would expect the hyperfine coupling constant [$^{115}A(1)$] at the In(1) site (Fig. 2a) of CeRh$_{0.5}$Ir$_{0.5}$In$_5$ to be smaller than that of the host material CeRhIn$_5$ because $^{115}A(1) = 25$ kOe μ_B^{-1} in CeRhIn$_5$ decreases with increasing pressure but becomes constant at $^{115}A(1) \sim 7$ kOe μ_B^{-1} above $P = 1$ GPa. Such a pressure-dependent $^{115}A(1)$ will affect the information inferred from $1/T_1$[34] and, therefore, it is important to determine $^{115}A(1)$ for CeRh$_{0.5}$Ir$_{0.5}$In$_5$ before proceeding to details of its T_1 results under pressure. Figure 2b shows the frequency-swept ^{115}In-nuclear magnetic resonance (NMR) spectra at a constant field. The spectrum is consistent with previously reported spectra of CeRhIn$_5$[34]. From these data, we establish the temperature dependence of the ^{115}In(1)-NMR center line plotted in Fig. 2c. With these results, we calculate (Methods) the temperature dependence of the Knight shift $^{115}K(1)_c$ (%) and compare it to dc susceptibility χ_c (emu mol^{-1}) in Fig. 2d. As clearly shown
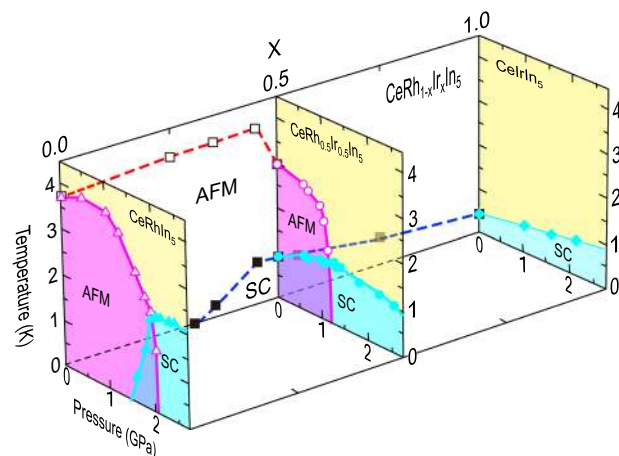

Fig. 1 Phase diagram of CeRh$_{1-x}$Ir$_x$In$_5$. x and pressure dependence of the Neel temperature T_N (open squares, triangles, and circles) and the superconducting transition temperature T_c (solid squares, triangles, circles, and diamonds) for CeRh$_{1-x}$Ir$_x$In$_5$ ($P = 0$)[19], CeRhIn$_5$[21–23], and CeIrIn$_5$[30] under pressure. AFM and SC indicate antiferromagnetic metal and superconductivity, respectively.
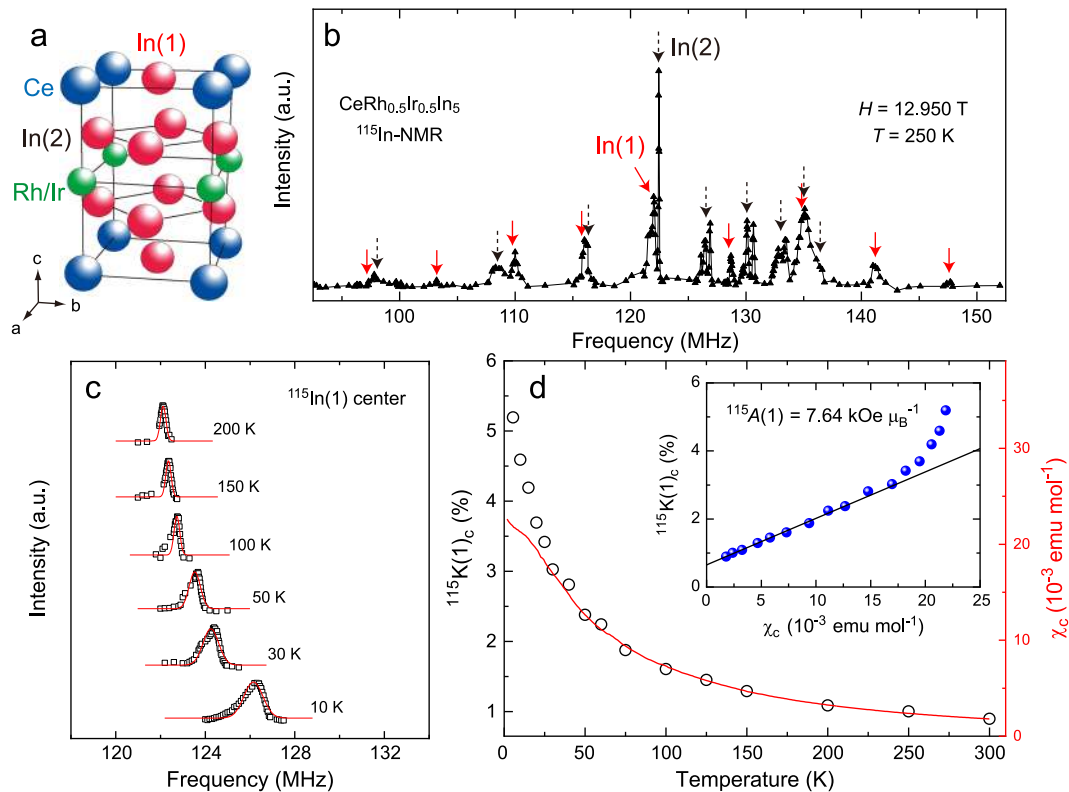
Fig. 2 Hyperfine coupling constant. a Crystal structure of $CeRh_{0.5}Ir_{0.5}In_5$. **b** Frequency-swept ^{115}In-nuclear magnetic resonance (NMR) spectra of $CeRh_{0.5}Ir_{0.5}In_5$. Solid [dotted] arrows indicate In(1)[In(2)] resonance peaks, respectively. **c** Temperature dependence of the $^{115}In(1)$-NMR center line. The curves are Gaussian fits. **d** Temperature dependence of the Knight shift $^{115}K(1)_c$ (open circles) and dc susceptibility χ_c (solid curve). The inset shows $^{115}K(1)_c$ vs. χ_c. The solid straight line is a fit to the data above $T = 30$ K, which yields the hyperfine coupling constant $^{115}A(1) = 7.64$ kOe μ_B^{-1}. Error bars are smaller than the size of the data points.

in the figure, the relation $K(T) \propto {}^{115}A(1)\chi(T)$ holds above $T = 30$ K. A breakdown of this linear relationship at low temperature is common in heavy electron systems[35], but a previous In-NMR study suggested that $^{115}A(1)$ is temperature-independent in $CeIrIn_5$ in such temperature regime[36]. In the inset of Fig. 2d, we plot $^{115}K(1)_c$ vs. χ_c and obtain the hyperfine coupling constant as $^{115}A(1) = 7.64$ kOe μ_B^{-1}. This closely corresponds to the value of $^{115}A(1)$ in $CeRhIn_5$ under a pressure of 1 GPa (Supplementary Note 1 and Supplementary Fig. 1), and thus, it substantiates the suggestion that Ir substitution with $x = 0.5$ (chemical pressure) is equivalent to the application of a physical pressure greater than $P = 1$ GPa to $CeRhIn_5$. Therefore, we reasonably can ignore any significant pressure dependence of $^{115}A(1)$ in inferring the pressure evolution of physical properties from $1/T_1$ in $CeRh_{0.5}Ir_{0.5}In_5$.

Pressure dependence of T_N and T_c. Figure 3a and b shows the temperature dependence of $1/T_1$. The magnitude of $1/T_1$ for $CeRh_{0.5}Ir_{0.5}In_5$ is much greater than that for the nonmagnetic reference material $La(Rh,Ir)In_5$[37], due to f electron spin correlations, that are reflected in the dynamical susceptibility χ'' to which $1/T_1$ is proportional. At $P = 0$, $1/T_1$ exhibits a small peak at $T_N = 3.0$ K and decreases below $T_c = 0.9$ K[19]. As shown in Fig. 3a and the inset, $T_N(P)$ can be identified up to $P = 1.12$ GPa but disappears above $P_c^{AF} = 1.2$ GPa. A superconducting transition is observed at all pressures, as evidenced by an abrupt reduction of $1/T_1$ below $T = T_c(P)$. T_c increases with increasing pressure and exhibits a maximum $T_c^{max} = 1.4$ K around $P_c^{AF} = 1.2$ GPa and then decreases with further increase of P; T_c^{max} is 1.6 times higher than $T_c = 0.9$ K at $P = 0$.

Pressure dependence of the Kondo hybridization. To probe the character of f electrons as a function of pressure, we use the In(1) ^{115}In-NQR frequency ν_Q. In general, ν_Q is determined by the surrounding lattice and on-site electrons with the latter being dominant in strongly correlated electron systems[38]; in the current case the latter reflects f–c hybridization that generates an electric field gradient (EFG) at the In(1)-site, as was found in previous ^{115}In-NQR and NMR studies on $CeIn_3$[39] and $CeRhIn_5$[34] under pressure. Figure 4a–c shows the pressure dependence of the In(1) NQR spectrum and ν_Q (see Supplementary Note 2 and Supplementary Fig. 2 for detail). In general, ν_Q is expected to increase smoothly with decreasing volume[39]; however, this is not the case here. At $T = 4.2$ K, ν_Q weakly increases up to $P = 1.24$ GPa but jumps at $P^* = 1.35$ GPa above which the slope $d\nu_Q/dP$ increases by more than a factor of three. The same trend is found at lower temperatures where we see that P^* decreases as T is reduced. We denote the midpoint of the ν_Q jump in the P–T plane as $(P^*, T^*) = (1.35$ GPa, 4.2 K$)$, $(1.13$ GPa, 1.6 K$)$, and $(0.90$ GPa, 0.3 K$)$, respectively. The same result is also found in the In(2) site. Figure 4d, e shows the temperature dependence of the In(2) NQR spectrum and its peak position together with In(1) ν_Q at $P = 1.12$ GPa. As found in the In(1) site, the In(2) ν_Q increases below $T^* = 1.5$ K. In a previous study on $CeRhIn_5$, a similar change of EFG was found in the In(2) site at $P^* = 1.75$ GPa, although detailed pressure dependence for the In(1) site with a high accuracy was not conducted[34].

We consider the origin for the ν_Q jump. Figure 5a shows results of X-ray diffraction measurements that give the pressure dependence of a- and c-axis lengths; the lattice parameters decrease smoothly with increasing pressure to $P = 4$ GPa, without
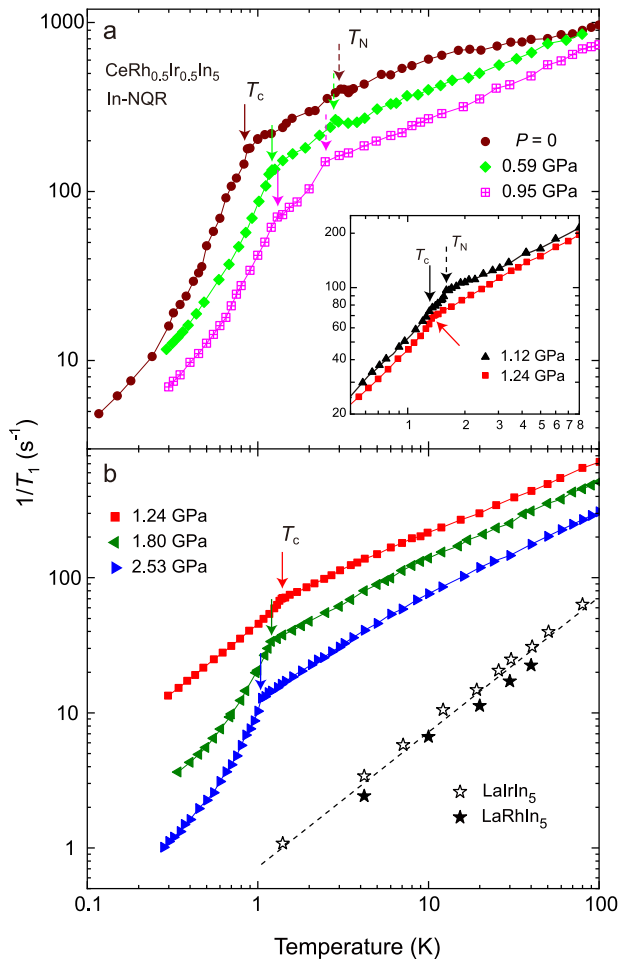
Fig. 3 Antiferromagnetism and superconductivity under pressure.
Temperature dependence of the In(1)-nuclear quadrupole resonance
(NQR) nuclear spin-lattice relaxation rate $1/T_1$ (**a**) below and (**b**) above the
antiferromagnetic (AF) quantum critical point P_c^{AF}. (Inset) Data for $P = 1.12$
and 1.24 GPa just around the Neel temperature T_N and the superconducting
transition temperature T_c. The dotted (solid) arrows indicate $T_N(T_c)$, while
the dashed line for La(Ir,Rh)In$_5$ indicates $1/T_1T =$ constant. Data at $P = 0$ [19]
and for La(Ir,Rh)In$_5$ are obtained from ref. [37]. Error bars are smaller than the
size of the data points.

any signature of a structural transition. From these data, we
calculate the EFG using the first-principles Hiroshima Linear-
Augmented-Plane-Wave (HiLAPW) codes[40]. As expected, the
calculated ν_Q^{HiLAPW} increases monotonically with applied pressure
(Fig. 5b). This and the lack of any anomaly in $1/T_1$ at (P^*, T^*) rule
out a change in lattice contribution to ν_Q as the origin of the ν_Q
jump. Furthermore, Fig. 5b compares the pressure dependence of
ν_Q^{HiLAPW} for CeRh(Ir)In$_5$ and LaRh(Ir)In$_5$. ν_Q^{HiLAPW} for CeRh(Ir)
In$_5$ is uniformly greater than that for LaRh(Ir)In$_5$, because CeRh
(Ir)In$_5$ has the additional EFG from hybridized f electrons, unlike
nonmagnetic LaRh(Ir)In$_5$. This result is consistent with previous
band calculations[41,42].

We conclude from these results that the jump in $\nu_Q(P)$ at $(P^*,
T^*)$ is due to a pronounced increase in Kondo hybridization at
(P^*, T^*) and that the larger $d\nu_Q/dP$ above (P^*, T^*) reflects that
increased hybridization. Because increased Kondo hybridization
transfers f spectral weight from localized to itinerant degrees of
freedom, and hence an increase in Fermi surface volume, the
pronounced jump in ν_Q signals the experimental observation of a
small (localized) to large (itinerant) Fermi surface. As the

principal axis of the EFG at the In(2) site is perpendicular to
that of the In(1) site, the ν_Q change at both sites suggests that the
entire Fermi-surface volume changes at (P^*, T^*).

Determination of the AF QCP. The temperature dependence of
T_1 just above $T \geq T_c(P)$ can be described by the self-consistent
renormalization (SCR) theory for spin fluctuations around an AF
QCP[43]. A three-dimensional AF spin fluctuation model is
applicable also to the low temperature thermopower S/T around
the pressure-induced AF QCP of CeRh$_{0.58}$Ir$_{0.42}$In$_5$[44]. Near an AF
QCP, the SCR model predicts $1/T_1T \propto \sqrt{\chi_Q(T)} = 1/\sqrt{T + \theta}$[43],
where $\chi_Q(T)$ is the Curie–Weiss staggered susceptibility and θ is
a measure of the distance to the AF QCP. At the QCP, $\theta = 0$
and $\chi_Q(T)$ diverges toward 0 K. $1/T_1T$ can be represented by the
sum of magnetic and small nonmagnetic contributions as $1/
T_1T = 1/(T_1T)_{AF} + 1/(T_1T)_{lattice}$. For the lattice term, we use the
mean value of $1/T_1T$ from reference materials LaRhIn$_5$ and
LaIrIn$_5$ (Fig. 3b), which gives $1/(T_1T)_{lattice} = 1.44$ (s^{-1} K^{-1}).

Figure 6a, b are plots of $1/T_1T$ vs. T for the AF phase below
$P = 1.12$ GPa and for the paramagnetic phase above $P = 1.24$
GPa, respectively. The solid curves in Fig. 6b are least-squares fits
to $1/T_1T = a/(T + \theta)^{0.5} + 1.44$ just above $T_c(P)$, with a and θ as
parameters. Approaching the AF QCP from $P = 2.53$ GPa, θ
decreases with decreasing pressure, as can be seen in Fig. 6b. The
pressure dependences of θ, T_N, and T_c are plotted in Fig. 6c. From
a linear fit of $\theta(P)$, the AF QCP ($\theta = 0$ K) for CeRh$_{0.5}$Ir$_{0.5}$In$_5$ is
obtained at $P_c^{AF} = 1.2$ GPa, where the highest T_c is realized. The
present results clearly indicate that spin fluctuations play a
significant role for superconductivity in CeRh$_{0.5}$Ir$_{0.5}$In$_5$.

Unconventional superconductivity at P_c^{AF}. As seen in Fig. 6a, b,
there is a strong pressure dependence of the magnitude of
$1/T_1T$ at the lowest temperatures of these measurements. To
place these results in perspective, we normalize $1/T_1T$ by its
value at T_c, $1/T_1T(T_c)$, and plot the ratio in Figs. 7a, b as a
function of reduced temperature $T/T_c(P)$. Deep in the super-
conducting state, this ratio is clearly largest at $P = 1.12$ GPa
near P_c^{AF} and depends only weakly on temperature below T_c.
This result contrasts with expectations for a fully gapped, e.g.,
s-wave, superconductor where $1/T_1$ should decrease exponen-
tially to a very small value well below T_c and for a clean d-wave
superconductor where $1/T_1$ decreases as T^3. In CeRh$_{0.5}$Ir$_{0.5}$In$_5$
at $P = 1.12$ GPa there must be a substantial fraction of low-
lying excitations in the normal state that remains ungapped
below T_c. Namely, $[T_1T(T = 0.3K)]^{-0.5}/[T_1T(T_c)]^{-0.5} =
N(E_F)^{residual}/N(E_F)^{normal}$ is the relative density of state (DOS) at
$T = 0.3$ K, which is consistent with the fraction of ungapped
quasiparticle DOS in the superconducting state.

To obtain the relative DOS, for simplicity we assume that T_1
below T_c is predominantly determined by itinerant quasi-
particles. Previously, an analysis within the context of two-fluid
phenomenological theory has deduced that the $4f$ local moments
also contribute to relaxation[45,46]. Nonetheless, as shown in
Supplementary Note 3 and Supplementary Figs. 3 and 4, such a
model reproduces essentially the same result as we obtained here.

Phase diagram. Figure 8a shows the pressure dependence of T_N
and T^* inferred from In(1) NQR, together with T_c on the P–T
plane. T^* inferred from In(2) NQR at $P = 1.12$ GPa coincides
with the result obtained from In(1). T^* extrapolates to zero at
$P_c^* = 0.8$ GPa, which is distinctly smaller than $P_c^{AF} = 1.2$ GPa. In
CeRhIn$_5$ ($x = 0$), a similar result was suggested with $P_c^* = 1.75$
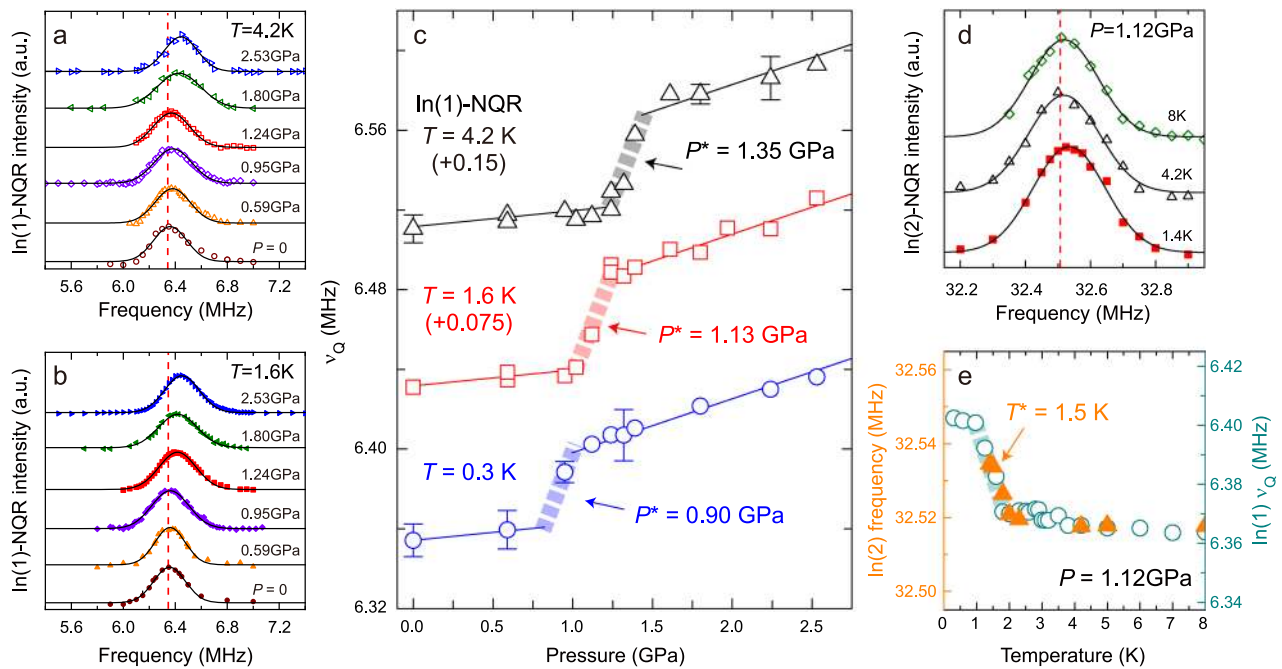GPa[34] and $P_c^{AF} = 2.1$ GPa[47]. Comparison of these critical

Fig. 4 Localized to itinerant transition. Pressure dependence of the In(1) ^{115}In-nuclear quadrupole resonance (NQR) spectrum ($\pm 1/2 \leftrightarrow \pm 3/2$ transition line) at $T = 4.2$ K (**a**) and 1.6 K (**b**). The curves are Gaussian fits. The dotted vertical lines indicate the peak positions at $P = 0$. **c** Pressure dependence of the NQR frequency (ν_Q) obtained at $T = 0.3$, 1.6, and 4.2 K. For clarity, the vertical axis for $T = 1.6$ and 4.2 K are offset by the amount shown in the parenthesis. Solid arrows indicate localized-to-itinerant transition pressure (P^*) which is defined from the midpoint of ν_Q jump. Solid straight lines are fits to the data which yield the slope $d\nu_Q/dP = 0.008$ (0.027) below (above) P^*. Error bars represent the uncertainty in estimating ν_Q. **d** Temperature dependence of the In(2) ^{115}In-NQR spectrum ($\pm 3/2 \leftrightarrow \pm 5/2$ transition line) at $P = 1.12$ GPa. The curves are Gaussian fits. Vertical line indicates the peak position at $T = 8$ K. **e** Temperature dependence of the peak position of the In(2) spectrum (solid triangles) and In(1) ν_Q (open circles) at $P = 1.12$ GPa. Solid arrow indicates localized-to-itinerant transition temperature T^* which is defined from the midpoint of ν_Q jump. The dashed line serves as visual guide. Error bars are smaller than the size of the data points except for those in (**c**).

pressure values shows that Ir substitution with $x = 0.5$ (chemical pressure) is effectively equivalent to the application of a physical pressure of about $P = 1$ GPa to CeRhIn$_5$. This conclusion is consistent with that drawn from our measurement of the hyperfine coupling presented earlier (Supplementary Note 1 and Supplementary Fig. 1). We emphasize again that, in the pressure regions we are interested for CeRhIn$_5$ and CeRh$_{0.5}$Ir$_{0.5}$In$_5$, ^{115}A (1) is constant, and thus changes in physical properties are not related to a changing hyperfine coupling but to the quantum criticality.

As shown in Fig. 8b, in CeRh$_{0.5}$Ir$_{0.5}$In$_5$, remarkably, the fraction of ungapped excitations strongly depends on pressure, reaching a maximum at the AF QCP. In the coexistent state at $P = 0$[19], this fraction is 50%, but increases to 96% at P_c^{AF} and then decreases to 55% with the increasing pressure at $P = 2.53$ GPa. The highest T_c around the AF QCP of CeRh$_{0.5}$Ir$_{0.5}$In$_5$ is realized unexpectedly with the largest fraction of gapless excitations. The present observation is completely different from that for CeRhIn$_5$ under pressure; in CeRhIn$_5$, the relative fraction of gapless excitations (88%) in the coexistent state is rapidly suppressed to almost zero as it approaches the QCP[47].

Discussion

From the phase diagram shown in Fig. 8, it is clear that the localized to itinerant transition ($T^*(P)$) does not occur exactly at the AF QCP; in the limit of zero temperature, P_c^* precedes P_c^{AF}. One possibility would be that the Fermi-surface change across the $T^*(P)$ boundary marks a line of abrupt changes of the Ce valence that terminates near $T = 0$ in a critical end point. A model that considers this possibility, however, appears to exclude the $T^*(P)$ boundary from extending into the AF state[48,49], contrary to our

results. In contrast, a breakdown of the Kondo effect gives rise to a small-to large Fermi surface change across $T^*(P)$[50]. This idea leads to a $T = 0$ phase diagram[16,51] similar to the results of Fig. 8. Associated with the Kondo breakdown and development of a large Fermi surface, soft charge fluctuations can emerge without a change in formal valence of Ce ions[52]. Within experimental uncertainty of $\pm 1.5\%$, there is no detectable difference between CeRhIn$_5$ and CeIrIn$_5$ at 10 K in their spectroscopically determined Ce valence[53], even though their Fermi volumes differ—a result that, together with the phase diagram of Fig. 8, supports a Kondo breakdown interpretation as do thermopower measurements on CeRh$_{0.58}$Ir$_{0.42}$In$_5$[44]. Notably, the T^* boundary has no notable effect on the evolution of $T_c(P)$. In passing, we mention a possibility of a more general case, a Lifshitz transition. Watanabe and Ogata[54], and Kuramoto et al.[55] pointed out that, even though the Kondo screening remains, a competition between the Kondo effect and the RKKY interaction can lead to a topological Fermi surface transition (Lifshitz transition) below the AF QCP[54,55], which is also consistent with our observation.

The large $1/T_1T$ below T_c at pressures near the AF QCP (Figs. 6 and 7) is quite remarkable, and its temperature independence implies a large DOS that remains ungapped in the superconducting state even though this is the pressure range where T_c is a maximum. Such an anomalously high value of ungapped DOS in the superconducting state has never been found in other QCP materials such as high T_c cuprates[56] and the iron-pnictide superconductors[5,57], even though magnetic fluctuations are also strong around their QCP. For the Ce115 family, no significant gapless excitations have been observed so far around a QCP[58].

In general, gapless excitations are expected from impurity scattering in d-wave superconductors[59–62]. Though there are no
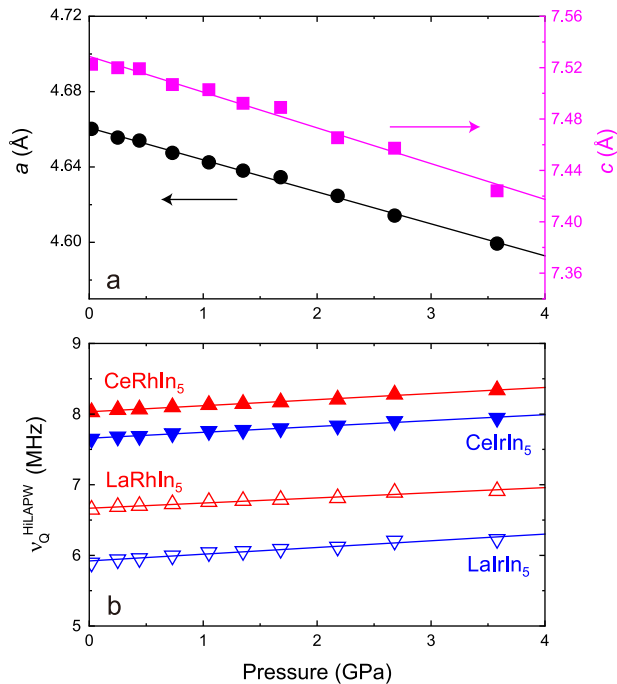
Fig. 5 Lattice parameters and band calculation. a Pressure dependence of a- and c-axis lengths for CeRh$_{0.5}$Ir$_{0.5}$In$_5$ at room temperature. **b** Pressure dependence of the nuclear quadrupole resonance frequency ν_Q^{HiLAPW} obtained from band calculations [Hiroshima Linear-Augmented-Plane-Wave (HiLAPW) code] for CeRh(Ir)In$_5$ and LaRh(Ir)In$_5$. LaRh(Ir)In$_5$ corresponds to the $4f$-localized model of CeRh(Ir)In$_5$. Both are calculated with the same lattice constant. Error bars are smaller than the size of the data points.

intentionally added impurities in our crystal, the random replacement of 50 % Rh by Ir results in a broadening of the In(1) NQR line by a factor of ~5 compared to CeIrIn$_5$[19,27]. Such randomness increases the resistivity at 4 K (just above T_N) from ~4 μΩcm in CeRhIn$_5$ to over 20 μΩcm in CeRh$_{0.5}$Ir$_{0.5}$In$_5$[32]. Quantum critical fluctuations can further enhance that scattering[61] to make part of a multi-sheeted Fermi surface gapless[63]. Such scattering concomitantly leads to pair breaking, resulting in a large reduction of T_c[59–64], which is inconsistent with our observations. The relative DOS at the pressure-induced QCP is almost zero in CeRhIn$_5$[47] but is enhanced to 96% in CeRh$_{0.5}$Ir$_{0.5}$In$_5$ at P_c^{AF}. If we assume that the symmetry of CeRh$_{0.5}$Ir$_{0.5}$In$_5$ is also d-wave, T_c should be reduced to zero with such a significant residual DOS at E_F[65]. In contrast to this expectation, the maximum $T_c = 1.4$ K for CeRh$_{0.5}$Ir$_{0.5}$In$_5$ remains at 61% of $T_c = 2.3$ K for CeRhIn$_5$ at their respective QCPs. Hence, the present results suggest that superconductivity near P_c^{AF} in CeRh$_{0.5}$Ir$_{0.5}$In$_5$ is more exotic than d-wave.

Model calculations of superconductivity in a two-dimensional Kondo lattice show that near an AF QCP d- and p-wave spin-singlet superconducting states are nearly degenerate, with an odd frequency p-wave spin-singlet state being favored when entering the large Fermi surfaces region to take advantage of the nesting condition with the vector $\mathbf{Q} = (\pi, \pi)$[66]. A p-orbital wave function with spin-singlet pairing symmetry satisfies Fermi statistics in the odd-frequency channel[67–70], and this odd-frequency pairing is more robust against nonmagnetic impurity scattering than even-frequency pairing[71]. Indeed, for a scattering strength that kills d-wave superconductivity completely, spin-singlet odd-frequency pairing will survive with a T_c that is approximately 60% of that in the absence of scattering[71]. Motivated by these theoretical results,

we suggest that odd-frequency spin-singlet pairing is realized in CeRh$_{0.5}$Ir$_{0.5}$In$_5$ in the vicinity of its critical pressures. Its robust T_c in the presence of substantial disorder scattering that gives rise to a large residual density of states at P_c^{AF} where quantum critical fluctuations are strongest and the presence of a nearby change from small-to large Fermi surface at P_c^* are fully consistent with our proposal. We stress that the unique aspect of both strong fluctuations and large Fermi surface is not shared by the end members, CeIrIn$_5$ or CeRhIn$_5$. Knight shift and experiments that directly probe the gap symmetry will be useful to test this possibility.

In summary, we reported systematic ^{115}In-NQR measurements on the heavy fermion AF superconductor CeRh$_{0.5}$Ir$_{0.5}$In$_5$ under pressure and find that an AF QCP is located at $P_c^{AF} = 1.2$ GPa, at which $T_c(P)$ reaches its maximum. The pressure and temperature dependence of ν_Q reveal a pronounced increase in hybridization that signals a change from small-to large Fermi surface in the limit of zero temperature at $P_c^* = 0.8$ GPa which is notably lower than P_c^{AF}. Thus, our work sheds new light on the quantum phase transition in f-electron systems. There is a strong enhancement of the quasiparticle DOS in the superconducting state around P_c^{AF} where the Fermi surface is large. The robustness of T_c under these conditions can be understood if the superconductivity is odd-frequency p-wave spin singlet. Traditionally, Hall coefficient and quantum oscillation experiments have been used to probe the Fermi surface change. Our work demonstrates that the NQR frequency can be used as a powerful tool to examine the change in Fermi surface volume for heavy electron systems. In particular, the NQR technique does not require single crystals and is not limited by sample quality or pressure, and thus will open a new venue to understand strongly correlated electron superconductivity.

Methods

Samples. Single crystals of CeRh$_{0.5}$Ir$_{0.5}$In$_5$ were grown from an In flux as reported in a previous study[18]. All experiments were performed with the same batch of crystals used in the previous NQR study[19]. As documented in detail in ref. [19], there is no phase separation into Rh-rich and Ir-rich parts even in the coarsely crushed powder. In fact, no excess peaks in the NMR/NQR spectrum are found and the spectrum can be reproduced by a Gaussian function. Moreover, T_1 is of single component, which also indicates that Ir is randomly distributed. For NMR Knight shift measurements, two single crystals, sized 2 mm—4 mm—0.5 mm and 2 mm—3 mm—0.4 mm, were used. For NQR measurements, the crystals were moderately crushed into grains to allow RF pulses to penetrate easily into the samples. Small and thin single-crystal platelets cleaved from an as-grown ingot were used for X-ray and dc-susceptibility measurements.

NQR measurement. For NQR, the nuclear spin Hamiltonian can be expressed as, $\mathcal{H}_Q = (h\nu_Q/6)[3I_z^2 - I(I+1) + \eta(I_x^2 - I_y^2)]$, where h is Planck's constant and $I = 9/2$ for the In nucleus is the nuclear spin; ν_Q and the asymmetry parameter η are defined as $\nu_Q = \frac{3eQV_{zz}}{2I(2I-1)h}$ and, $\eta = \frac{V_{xx}-V_{yy}}{V_{zz}}$, respectively, and Q and $V_{\alpha\beta}$ are the nuclear quadrupole moment and EFG tensor, respectively. In CeRh$_{0.5}$Ir$_{0.5}$In$_5$, there are two inequivalent In sites, one in the CeIn [In(1)] layer and another in the (Rh,Ir) In$_4$ [In(2)] layer (see Fig. 2a). The principle axis of the EFG at the In(1) [In(2)] site is parallel [perpendicular] to the c-axis. The ^{115}In-NQR spectra for In(1) ± 1/2 ↔ ±3/2 transition line (Supplementary Note 2 and Supplementary Fig. 2), ±7/2 ↔ ±9/2 transition line (Supplementary Fig. 5), the In(2) ±3/2 ↔ ±5/2 transition line and T_1 for the In(1) site ($\eta = 0$) (Supplementary Note 4 and Supplementary Figs. 6 and 7) were obtained as reported in an earlier study[19,72]. Here, T_1 probes the dynamic spin susceptibility through the hyperfine coupling constant A_q as $1/T_1 \propto T\sum_q |A_q|^2 \chi''(\mathbf{q}, \omega_0)/\omega_0$, where ω_0 is the NQR frequency[73] and $\mathbf{q}$ is a wave vector for AF order and/or quantum critical fluctuation in CeRh$_{0.5}$Ir$_{0.5}$In$_5$. Meanwhile, 1/$T_1 \propto N(E_F)^2 k_B T$ holds in a Pauli paramagnetic metal, i.e., in a heavy Fermi liquid state (Korringa law). Here, $N(E_F)$ is the density of states at E_F.

A NiCrAl/BeCu piston-cylinder-type pressure-cell filled with Daphne (7474) oil was used. The T_c of Sn was measured to determine the pressure. Measurements below 1 K were performed using a ^{3}He refrigerator.

X-ray measurement. A diamond anvil cell filled with a CeRh$_{0.5}$Ir$_{0.5}$In$_5$ single crystal and Daphne oil were used for room temperature X-ray measurements under pressure; the pressure was determined by measuring the fluorescence of ruby. All measurements were made at zero-magnetic field.
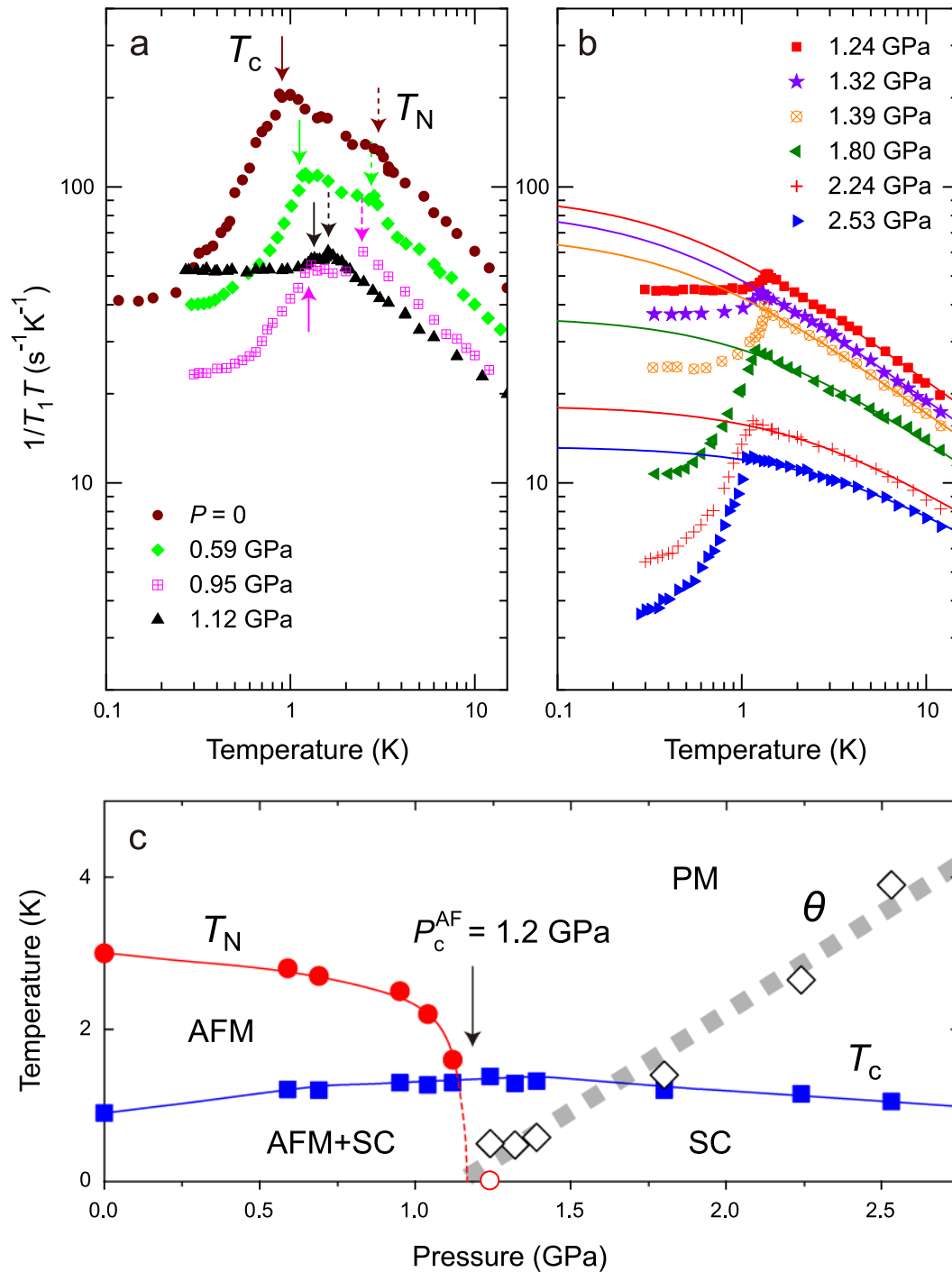
Fig. 6 Antiferromagnetic (AF) quantum critical point (P_c^{AF}). Temperature dependence of the nuclear spin-lattice relaxation rate divided by temperature $1/T_1T$ below (**a**) and above (**b**) P_c^{AF} with the fitting curves (see text). The dotted (solid) arrows indicate the Neel temperature T_N (the superconducting transition temperature T_c). **c** Summary of pressure dependence of the characteristic temperature θ (see text), T_N, and T_c. The dotted straight line (filled diamonds) is a fit to the data which yields P_c^{AF} ($\theta = 0$) = 1.2 GPa. PM and AFM indicate paramagnetic and antiferromagnetic metal, respectively. SC indicates superconductivity. Error bars are smaller than the size of the data points.

EFG calculation. The EFG is calculated using the all electron full-potential linear augmented plane wave method implemented in the Hiroshima Linear-Augmented-Plane-Wave (HiLAPW) code with generalized gradient approximation including spin–orbit coupling[40].

Hyperfine coupling constant. To estimate the hyperfine coupling constant for CeRh$_{0.5}$Ir$_{0.5}$In$_5$, $^{115}A(1)$, we measure the ^{115}In(1)-NMR spectrum and dc susceptibility. For NMR, the nuclear spin Hamiltonian is expressed as $\mathcal{H} = -^{115}\gamma\hbar\mathbf{I}\cdot\mathbf{H}(1+K) + \mathcal{H}_Q$, where the gyromagnetic ratio $^{115}\gamma = 9.3295$ MHz T^{-1}, $\mathbf{H}$ is the

external magnetic field, and K is the Knight shift. ^{115}In-NMR spectra have nine transitions from $I_z = (2m+1)/2$ to $(2m-1)/2$ where $m = -4, -3, -2, -1, 0, 1, 2, 3, 4$ for In(1) and In(2) sites, respectively, with K, ν_Q, and η as parameters. At ambient pressure, ν_Q and η at the In(1) [In(2)] site are 6.35 MHz (17.37 MHz) and 0 (0.473), respectively[19]. The Knight shift for In(1), $^{115}K(1)_c(T)$, was calculated from the peak in the ^{115}In(1)-NMR center line ($m = 0$) taken by sweeping the RF frequency at a fixed field $H = 12.950$ T and χ_c (emu mol^{-1}) is obtained by dc susceptibility measurements at $H = 3$ T using a superconducting quantum interference device with the vibrating sample magnetometer. The magnetic field H is fixed perpendicular to the CeIn layer (c-axis).
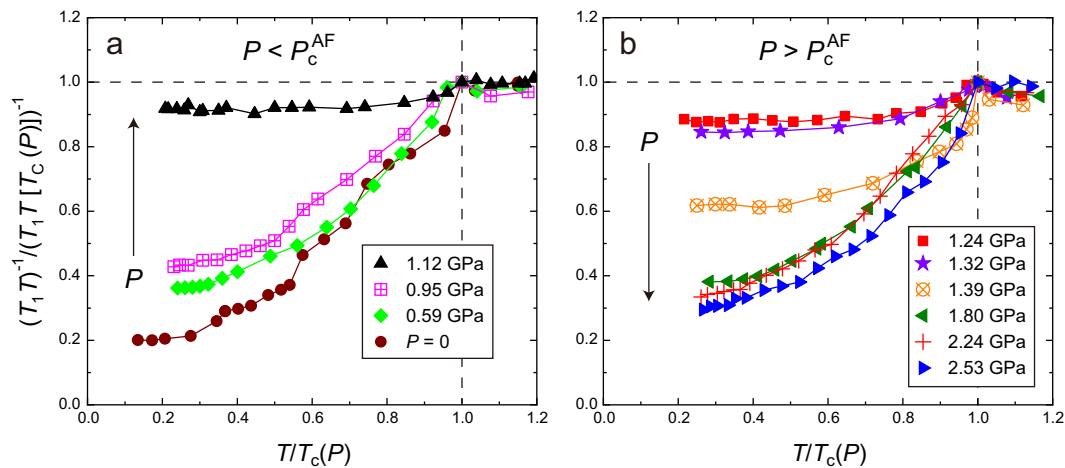
Fig. 7 Low-lying excitations in the superconducting state. Temperature dependence of the nuclear spin-lattice relaxation rate divided by temperature $1/T_1T$ below (**a**) and above (**b**) the antiferromagnetic (AF) quantum critical point (P_c^{AF}). Data at $P = 0$ are obtained from the literature[19]. Horizontal and vertical axes are normalized by the superconducting transition temperature $T_c(P)$ and $1/T_1T[T_c(P)]$, respectively. Error bars are smaller than the size of the data points.
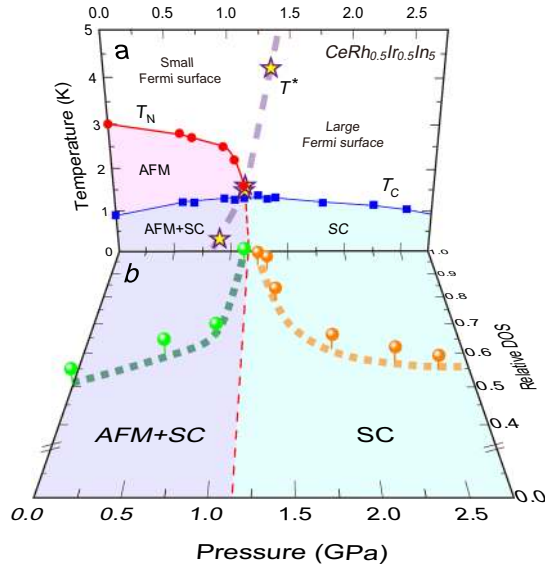

Fig. 8 Phase diagram. a Pressure–temperature phase diagram for $CeRh_{0.5}Ir_{0.5}In_5$ obtained at zero-magnetic field. The solid circles, squares, and stars indicate the Neel temperature T_N, the superconducting transition temperature T_c, and the localized-to-itinerant transition temperature T^*, respectively. The broken curve is a phase boundary separating small and large Fermi surfaces. **b** Pressure dependence of the relative density of states (DOS) on the $T = 0.3$ K plane. The dotted straight line indicates the antiferromagnetic (AF) quantum critical point ($P_c^{AF} = 1.2$ GPa). The solid and dashed curves serve as visual guides. AFM and SC indicate antiferromagnetic metal and superconductivity, respectively. Error bars are smaller than the size of the data points.

Data availability

The data that support the findings of this study are available on reasonable request. Correspondence and requests for materials should be addressed to G.-Q.Z.

References

1. Mathur, N. D., Grosche, F. M., Julian, S. R., Walker, I. R. & Freye, D. M. et al. Magnetically mediated superconductivity in heavy fermion compounds. *Nature* **394**, 39–43 (1998).
2. Löhneysen, Hv, Pietrus, T., Portisch, G., Schlager, H. G., Schröder, A. & Sieck, M. et al. Non-Fermi-liquid behavior in a heavy-fermion alloy at a magnetic instability. *Phys. Rev. Lett.* **72**, 3262–3265 (1994).
3. Abanov, A., Chubukov, A. V. & Schmalian, J. Quantum-critical theory of the spin-fermion model and its application to cuprates: normal state analysis. *Adv. Phys.* **52**, 119–218 (2003).
4. Abrahams, E. & Si, Q. Quantum criticality in the iron pnictides and chalcogenides. *J. Phys.* **23**, 223201 (2011).
5. Zhou, R., Li, Z., Yang, J., Sun, D. L. & Lin, C. T. et al. Quantum criticality in electron-doped $BaFe_{2-x}Ni_xAs_2$. *Nat. Commun.* **4**, 2265 (2013).
6. Luo, J., Yang, J., Zhou, R., Mu, Q. G. & Liu, T. et al. Tuning the distance to a possible ferromagnetic quantum critical point in $A_2Cr_3As_3$. *Phys. Rev. Lett.* **123**, 047001 (2019).
7. Hertz, J. A. Quantum critical phenomena. *Phys. Rev. B* **14**, 1165–1184 (1976).
8. Moriya, T. *Spin Fluctuations in Itinerant Electron Magnetism, Springer Series in Solid-State Sciences*. (Springer, Berlin), Vol. 56 (1985).
9. Millis, A. J. Effect of a nonzero temperature on quantum critical points in itinerant fermion systems. *Phys. Rev. B* **48**, 7183–7196 (1993).
10. Si, Q. & Steglich, F. Heavy Fermions and quantum. *Phase Transit. Sci.* **329**, 1161–1166 (2010).
11. Doniach, S. The Kondo lattice and weak antiferromagnetism. *Phys. B* **91**, 231–234 (1977).
12. Chen, Q. Y., Xu, D. F., Niu, X. H., Jiang, J. & Peng, R. et al. Direct observation of how the heavy-fermion state develops in $CeCoIn_5$. *Phys. Rev. B* **96**, 045107 (2017).
13. Chen, Q. Y., Xu, D. F., Niu, X. H., Peng, R. & Xu, H. C. et al. Band dependent interlayer f-electron hybridization in $CeRhIn_5$. *Phys. Rev. Lett.* **120**, 066403 (2018).
14. Burdin, S., Georges, A. & Grempel, D. R. Coherence scale of the Kondo lattice. *Phys. Rev. Lett.* **85**, 1048–1051 (2000).
15. Si, Q., Rabello, S., Ingersent, K. & Smith, J. L. Locally critical quantum phase transitions in strongly correlated metals. *Nature* **413**, 804–808 (2001).
16. Coleman, P. & Nevidomskyy, A. H. Frustration and the Kondo effect in heavy fermion materials. *J. Low. Temp. Phys.* **161**, 182–202 (2010).
17. Löhneysen, H. V., Rosch, A., Vojta, M. & Wölfle, P. Fermi-liquid instabilities at magnetic quantum phase transitions. *Rev. Mod. Phys.* **79**, 1015–1075 (2007).
18. Pagliuso, P. G., Petrovic, C., Movshovich, R., Hall, D. & Hundley, M. F. et al. Coexistence of magnetism and superconductivity in $CeRh_{1-x}Ir_xIn_5$. *Phys. Rev. B* **64**, 100503(R) (2001).
19. Zheng, G.-Q., Yamaguchi, N., Kan, H., Kitaoka, Y. & Sarrao, J. L. et al. Coexistence of antiferromagnetic order and unconventional superconductivity in heavy-fermion $CeRh_{1-x}Ir_xIn_5$ compounds: nuclear quadrupole resonance studies. *Phys. Rev. B* **70**, 014511 (2004).

20. Shishido, H., Settai, R., Harima, H. & Ōnuki, Y. A drastic change of the Fermi surface at a critical pressure in CeRhIn$_5$: dHvA study under pressure. *J. Phys. Soc. Jpn* **74**, 1103–1106 (2005).

21. Hegger, H., Petrovic, C., Moshopoulou, E. G., Hundley, M. F. & Sarrao, J. L. et al. Pressure-induced superconductivity in quasi-2D CeRhIn$_5$. *Phys. Rev. Lett.* **84**, 4986–4989 (2001).

22. Park, T., Ronning, F., Yuan, H. Q., Salamon, M. B. & Movshovich, R. et al. Hidden magnetism and quantum criticality in the heavy fermion superconductor CeRhIn$_5$. *Nature* **440**, 65–68 (2006).

23. Knebel, G., Aoki, D., Braithwaite, D., Salce, B. & Flouquet, J. Coexistence of antiferromagnetism and superconductivity in CeRhIn$_5$ under high pressure and magnetic field. *Phys. Rev. B* **74**, 020501(R) (2006).

24. Mito, T., Kawasaki, S., Zheng, G.-Q., Kawasaki, Y. & Ishida, K. et al. Pressure-induced anomalous magnetism and unconventional superconductivity in CeRhIn$_5$: ^{115}In-NQR study under pressure. *Phys. Rev. B* **63**, 220507(R) (2001).

25. Park, T., Bauer, E. D. & Thompson, J. D. Probing the nodal gap in the pressure-induced heavy fermion superconductor CeRhIn$_5$. *Phys. Rev. Lett.* **101**, 177002 (2008).

26. Shishido, H., Settai, R., Aoki, D., Ikeda, S. & Nakawaki, H. et al. Fermi surface, magnetic and superconducting properties of LaRhIn$_5$ and CeTIn$_5$ (T: Co, Rh and Ir). *J. Phys. Soc. Jpn.* **71**, 162–173 (2002).

27. Zheng, G.-Q., Tanabe, K., Mito, T., Kawasaki, S. & Kitaoka, Y. et al. Unique spin dynamics and unconventional superconductivity in the layered heavy Fermion compound CeIrIn$_5$: NQR evidence. *Phys. Rev. Lett.* **86**, 4664–4667 (2001).

28. Lu, X., Lee, H., Park, T., Ronning, F. & Bauer, E. D. et al. Heat-capacity measurements of energy-gap nodes of the heavy-Fermion superconductor CeIrIn$_5$ deep inside the pressure-dependent dome structure of its superconducting phase diagram. *Phys. Rev. Lett.* **108**, 027001 (2012).

29. Petrovic, C., Movshovich, R., Jaime, M., Pagliuso, P. G. & Hundley, M. F. et al. A new heavy-fermion superconductor CeIrIn$_5$: a relative of the cuprates ? *Eur. Phys. Lett.* **53**, 354–359 (2001).

30. Kawasaki, S., Zheng, G.-Q., Kan, H., Kitaoka, Y. & Shishido, H. et al. Enhancing the superconducting transition temperature of the heavy Fermion compound CeIrIn$_5$ in the absence of spin correlations. *Phys. Rev. Lett.* **94**, 037007 (2005).

31. Christianson, A. D., Llobet, A., Bao, W., Gardner, J. S. & Swainson, I. P. et al. Novel coexistence of superconductivity with two distinct magnetic orders. *Phys. Rev. Lett.* **95**, 217002 (2005).

32. Nicklas, M., Sidorov, V. A., Borges, H. A., Pagliuso, P. G. & Sarrao, J. L. et al. Two superconducting phases in CeRh$_{1-x}$Ir$_x$In$_5$. *Phys. Rev. B* **70**, 020505(R) (2004).

33. Willers, T., Strigari, F., Hu, Z., Sessi, V. & Brookes, N. B. et al. Correlation between ground state and orbital anisotropy in heavy Fermion materials. *Proc. Natl Acad. Sci. USA* **112**, 2384–2388 (2015).

34. Lin, C. H., Shirer, K. R., Crocker, J., Dioguardi, A. P. & Lawson, M. M. et al. Evolution of hyperfine parameters across a quantum critical point in CeRhIn$_5$. *Phys. Rev. B* **92**, 155147 (2015).

35. Curro, N. J., Young, B.-L., Schmalian, J. & Pines, D. Scaling in the emergent behavior of heavy-electron materials. *Phys. Rev. B* **70**, 235117 (2004).

36. Kambe, S., Tokunaga, Y., Sakai, H. & Chudo, H. et al. One-component description of magnetic excitations in the heavy-fermion compound CeIrIn$_5$. *Phys. Rev. B* **81**, 140405(R) (2010).

37. Zheng, G.-Q., Kawasaki, S., Yamaguchi, N., Tanabe, K. & Mito, T. et al. Magnetism and superconductivity in CeRhIn$_5$ under chemical and hydrostatic pressures. *Phys. B* **329–333**, 450–451 (2003).

38. Zheng, G.-Q., Kitaoka, Y., Ishida, K. & Asayama, K. Local hole distribution in the CuO$_2$ plane of high-T_c Cu-oxides studied by Cu and oxygen NQR/NMR. *J. Phys. Soc. Jpn.* **64**, 2524–2532 (1995).

39. Kawasaki, S., Yashima, M., Kitaoka, Y., Takeda, K. & Shimizu, K. et al. Pressure-induced unconventional superconductivity in the heavy-fermion antiferromagnet CeIn$_3$: an ^{115}In-NQR study under pressure. *Phys. Rev. B* **77**, 064508 (2008).

40. Oguchi, T. Electronic band structure and structural stability of LaBiPt. *Phys. Rev. B* **63**, 125115 (2001).

41. Betsuyaku, K. & Harima, H. Electronic structure and electric field gradient of RIn$_3$ and RTIn$_5$ (R = La and Ce, T = Co, Rh and Ir). *J. Magn. Magn. Mater.* **272–276**, 187–188 (2004).

42. Rusz, J., Oppeneer, P. M., Curro, N. J., Urbano, R. R. & Young, B.-L. et al. Probing the electronic structure of pure and doped CeMIn$_5$ (M =Co,Rh, Ir) crystals with nuclear quadrupolar resonance. *Phys. Rev. B* **77**, 245124 (2008).

43. Moriya, T. & Ueda, K. Antiferromagnetic spin fluctuation and superconductivity. *Rep. Prog. Phys.* **66**, 1299–1341 (2003).

44. Luo, Y. K., Lu, X., Dioguardi, A. P., Rosa, P. F. S. & Bauer, E. D. et al. Unconventional and conventional quantum criticalities in CeRh$_{0.58}$Ir$_{0.42}$In$_5$. *npj Quant. Mater.* **3**, 6 (2018).

45. Yang, Y.-F., Urbano, R., Curro, N. J., Pines, D. & Bauer, E. D. Magnetic excitations in the Kondo liquid: superconductivity and hidden magnetic quantum critical fluctuations. *Phys. Rev. Lett.* **103**, 197004 (2009).

46. Yang, Y.-F. & Pines, D. Emergent states in heavy-electron materials. *Proc. Natl Acad. Sci. USA* **109**, E3060–E3066 (2012).

47. Yashima, M., Kawasaki, S., Mukuda, H., Kitaoka, Y. & Shishido, H. et al. Quantum phase diagram of antiferromagnetism and superconductivity with a tetracritical point in CeRhIn$_5$ in zero magnetic field. *Phys. Rev. B* **76**, 020509 (R) (2007).

48. Watanabe, S. & Miyake, K. Origin of drastic change of fermi surface and transport anomalies in CeRhIn$_5$ under pressure. *J. Phys. Soc. Jpn.* **79**, 033707 (2010).

49. Miyake, K. & Watanabe, S. Unconventional quantum criticality due to critical valence transition. *J. Phys. Soc. Jpn.* **83**, 061006 (2014).

50. Si, Q., Rabello, S., Ingersent, K. & Smith, J. L. Local fluctuations in quantum critical metals. *Phys. Rev. B* **68**, 115103 (2003).

51. Si, Q. Global magnetic phase diagram and local quantum criticality in heavy fermion metals. *Phys. B* **378-380**, 23–27 (2006).

52. Komijani, Y. & Coleman, P. Emergent critical charge fluctuations at the Kondo breakdown of heavy fermions. *Phys. Rev. Lett.* **122**, 217001 (2019).

53. Sundermann, M., Strigari, F., Willers, T., Weinen, J. & Liao, Y. F. et al. Quantitative study of the f occupation in CeMIn$_5$ and other cerium compounds with hard X-rays. *J. Elect. Spectr. Rel. Phenom.* **209**, 1–8 (2016).

54. Watanabe, H. & Ogata, M. Fermi-surface reconstruction without breakdown of Kondo screening at the quantum critical point. *Phys. Rev. Lett.* **99**, 136401 (2007).

55. Kuramoto, Y. & Hoshino, S. Composite Orders and Lifshitz transition of heavy electrons. *J. Phys. Soc. Jpn.* **83**, 061007 (2014).

56. Asayama, K., Kitaoka, Y., Zheng, G.-Q. & Ishida, K. NMR studies of high T_c superconductors. *Prog. Nucl. Magn. Reson. Spectrosc.* **28**, 221–253 (1996).

57. Oka, T., Li, Z., Kawasaki, S., Chen, G. F. & Wang, N. L. et al. Antiferromagnetic spin fluctuations above the dome-shaped and full-gap superconducting states of LaFeAsO$_{1-x}$F$_x$ revealed by ^{75} as-nuclear quadrupole resonance. *Phys. Rev. Lett.* **108**, 047001 (2012).

58. Kohori, Y., Yamato, Y., Iwamoto, Y., Kohara, T. & Bauer, E. D. et al. NMR and NQR studies of the heavy fermion superconductors CeTIn$_5$ (T = Co and Ir). *Phys. Rev. B* **64**, 134526 (2001).

59. Schmitt-Rink, S., Miyake, K. & Varma, C. M. Transport and thermal properties of heavy-fermion superconductors: a unified picture. *Phys. Rev. Lett.* **57**, 2575–2578 (1986).

60. Hirschfeld, P., Vollhardt, D. & Wölfle, P. Resonant impurity scattering in heavy fermion superconductors. *Solid State Commun.* **59**, 111–115 (1986).

61. Miyake, K. & Maebashi, H. A route to small Drude weight in metals with nested spin fluctuations and enhanced impurity scattering associated with quantum critical phenomena. *J. Phys. Chem. Solids* **62**, 53–57 (2011).

62. Haas, S., Balatsky, A. V., Sigrist, M. & Rice, T. M. Extended gapless regions in disordered $d_{x^2-y^2}$ wave superconductors. *Phys. Rev. B* **56**, 5108–5111 (1997).

63. Barzykin, V. & Gor'kov, L. P. Gapless Fermi surfaces in superconducting CeCoIn$_5$. *Phys. Rev. B* **76**, 014509 (2007).

64. Abrikosov, A. & Gor'kov, L. P. Contribution to the theory of superconducting alloys with paramagnetic impurities. *Sov. Phys. JETP* **12**, 1243 (1961).

65. Puchkaryov, E. & Maki, K. Impurity scattering in d-wave superconductivity. Unitarity limit versus Born limit. *Eur. Phys. J. B* **4**, 191–194 (1998).

66. Otsuki, J. Competing d-wave and p-wave spin-singlet superconductivities in the two-dimensional Kondo lattice. *Phys. Rev. Lett.* **115**, 036404 (2015).

67. Balatsky, A. & Abrahams, E. New class of singlet superconductors which break time reversal and parity. *Phys. Rev. B* **45**, 13125(R) (1992).

68. Coleman, P., Miranda, E. & Tsvelik, A. Possible realization of odd-frequency pairing in heavy fermion compounds. *Phys. Rev. Lett.* **70**, 2960–2963 (1993).

69. Fuseya, Y., Kohno, H. & Miyake, K. Realization of odd-frequency p-wave spin-singlet superconductivity coexisting with antiferromagnetic order near quantum critical point. *J. Phys. Soc. Jpn.* **72**, 2914–2923 (2003).

70. Berezinskii, V. L. New model of the anisotropic phase of superfluid ^{3} He. *JETP Lett.* **20**, 287 (1974).

71. Yoshioka, Y. & Miyake, K. Impurity effect on frequency dependent superconductivity: odd-frequency pairing and even-frequency pairing. *J. Phys. Soc. Jpn.* **81**, 093702 (2012).

72. MacLaughlin, D. E., Williamson, J. D. & Butterworth, J. Nuclear spin-lattice relaxation in pure and impure indium. I. Normal state. *Phys. Rev. B* **4**, 60–70 (1971).

73. Moriya, T. The effect of electron-electron interaction on the nuclear spin relaxation in metals. *J. Phys. Soc. Jpn.* **18**, 516–520 (1963).

Author contributions

G.-Q.Z. planned the project. J.L.S. and J.D.T. synthesized the single crystal. S.K., T.O., A.S., Y.K., and K.U. performed NQR measurements. S.K and Y.K. performed the NMR and susceptibility measurements. J.G., S.C., and L.L.S. performed the X-ray measurement. K.M. performed the band structure calculation. G.-Q.Z., S.K., and J.D.T. wrote the paper. All authors discussed the results and interpretation.

Competing interests

The authors declare no competing interests.

Additional information

Supplementary information is available for this paper at https://doi.org/10.1038/s42005-020-00418-x.

Correspondence and requests for materials should be addressed to S.K. or G.-q.Z.

Reprints and permission information is available at http://www.nature.com/reprints

Publisher's note Springer Nature remains neutral with regard to jurisdictional claims in published maps and institutional affiliations.